Stereoregular Diblock Copolymers of Syndiotactic Polypropylene and Polyesters: Syntheses and Self-Assembled Nanostructures

ARTICLE *in* MACROMOLECULES · APRIL 2009

Impact Factor: 5.8 · DOI: 10.1021/ma802598n

8 AUTHORS, INCLUDING:

Ming-Siao Hsiao
Air Force Research Laboratory, WPAFB
22 PUBLICATIONS **307** CITATIONS

Stereoregular Diblock Copolymers of Syndiotactic Polypropylene and Polyesters: Syntheses and Self-Assembled Nanostructures

Fu-Yuan Tzeng,[†] Ming-Champ Lin,[‡] Jheng-Yuan Wu,[†] Jing-Chung Kuo,[†] Jing-Cherng Tsai,*[,†] Ming-Siao Hsiao,[§] Hsin-Lung Chen,*[,‡] and Stephen Z. D. Cheng[§]

Department of Chemical Engineering, National Chung Cheng University, Chia-Yi 62142, Taiwan, Department of Chemical Engineering, National Tsing Hua University, Hsinchu 30013, Taiwan, and Maurice Morton Institute and Department of Polymer Science, The University of Akron, Akron, Ohio 44325-3909

Received November 21, 2008; Revised Manuscript Received March 6, 2009

ABSTRACT: Structurally well-defined stereoregular diblock copolymers composing of syndiotactic polypropylene (sPP) and polyester have been prepared using controlled ring-opening copolymerization of cyclic esters, including ε-caprolactone and DL-lactide, mediated by aluminum alkoxide end-capped sPP as the macroinitiator. The aluminum alkoxide end-capped sPP was generated by the in situ activation of hydroxyl-capped sPP with triethylaluminum (TEA). The hydroxy-capped sPP was prepared via the selective chain transfer reaction to TEA while inducing the syndiospecific polymerization of propylene in the presence of *ansa*-metallocene catalysts. The synthetic method not only offers high-yield production of the stereoregular block copolymers but also provides successful linking of the stereoregular polyolefins with an abundant variety of polymers as the second block. Moreover, the synthetic method offers effective control over the block chain length and molecular weight distribution; thus, the microphase separation of the resultant diblock copolymers generated well-ordered nanostructures as revealed by small-angle X-ray scattering.

Introduction

Block copolymers (BCPs) formed by the covalent linkage of two or more chemically distinct polymers at their chain ends[1] are known to self-organize[2] in the melt or solution state to form long-range ordered nanopatterns[3] that may have diverse technological applications.[4] Incorporating crystallizable moieties within the BCPs has been demonstrated to increase the morphological richness and kinetic complexity in the self-assembly process.[5] In particular, the microphase-separated morphology in the melt may be perturbed depending on the relative values of the order−disorder transition temperature (T_{ODT}), the crystallization temperature (T_c), and the glass transition temperature of the amorphous block (T_g^A). Considering the conventional crystalline−amorphous diblock copolymers, if T_c falls between T_{ODT} and T_g^A, the amorphous phase remains soft during the crystallization of the crystalline block; in this case, the melt mesophase may be strongly perturbed by the crystallization process and the extent of structure perturbation is governed by the segregation strength.[6−10] For $T_{ODT} > T_g^A > T_c$ (where the amorphous phase is in the glassy state) the crystallization can be effectively confined within the corresponding microdomains predetermined by the microphase segregation.[10−14] The crystallization behavior becomes even more complex if both blocks in the copolymer are crystallizable. Here the competition in the crystallization of the two components and the interplay of such a competition with the driving force of microphase separation should be the key that determines the crystalline morphology.[15−22]

Several crystalline polymers are known to possess steroregularity in their chain configurations. Recent reports have revealed that the incorporation of stereoregular segments into crystalline BCPs can result in the formation of unusual nanopatterns due to the stereointeraction between the stereoregular entities.[23] The prospect of simultaneous examination of the roles of stereointeraction and crystallization prompts us to develop new synthetic methods that offer the preparation of structurally well-defined stereoregular BCPs containing a crystallizable stereoregular block.

To date, stereoregular polyolefin-based BCPs have been prepared mainly by two synthetic routes: (i) living polymerization in the presence of stereospecific catalysts,[24] in which the block copolymers were generated directly by sequential polymerizations of different monomers, and (ii) utilization of stereoregular polymers with specific end groups (end-functionalized stereoregular prepolymers) that can be linked to the second block by postpolymerization.[25,26] Route i suffers the disadvantage that the variety of the block copolymers obtainable is extremely limited because of their preparation from sequential addition of structurally similar monomers to a single type of active species. Moreover, the similarity of the chemical structures of the monomers for the living polymerizations hamper the utilization of this synthetic route for preparing the stereoregular BCPs with sufficiently strong segregation strength between the constituting blocks for microphase separation.[1,24] By contrast, the preparations of stereoregular BCPs via postpolymerization of end-functionalized prepolymers (i.e., route ii) allows the stereoregular blocks to link with a broad variety of polymers as the second block. Nevertheless, stereoregular BCPs prepared by most of the prior postpolymerization methods failed to facilitate effective structural control for providing stereoregular BCPs with well-defined chemical structure; thus, the resulting stereoregular BCPs were unable to self-organize into consistent nanomorphologies.[25] The failure of these synthetic methods (via postpolymerization of end-functionalized prepolymer route) could be attributed to the difficulties encountered in the preparation of structurally well-defined stereoregular end-functionalized prepolymers and in providing a highly efficient linking method that facilitates the successful connection

* To whom correspondence should be addressed. (J.-C.T.) Telephone: 886-5-2720411 ext 33460. Fax: 886-5-2721206. E-mail chmjct@ccu.edu.tw. (H.-L.C.) Telephone: 886-3-5721714. Fax: 886-3-5738415. E-mail: hlchen@che.nhu.edu.tw.

[†] Department of Chemical Engineering, National Chung Cheng University.

[‡] Department of Chemical Engineering, National Tsing Hua University.

[§] Maurice Morton Institute and Department of Polymer Science, The University of Akron.

10.1021/ma802598n CCC: $40.75
Published on Web 04/03/2009

Table 1. Results of Selective Chain Transfer Reaction Studies by Conducting Propylene Polymerization in the Presence of Various Alkylaluminums and *ansa*-Metallocene Catalysts[a]

										end group ratio(%)[g]	
run	catalyst[b]	AlR_3[c]	AlR_3 (mmol)	pressure (atm)	temp (°C)	activity[d]	M_n[e]	PDI[e]	T_m[f] (°C)	hydroxyl	vinylidene
1	**I**	TMA	3	0.6	20	620	40200	2.04	129.9	86.36	13.64
2	**I**	TMA	6	0.6	20	512	20100	2.11	125.5	90.74	9.26
3	**I**	TMA	9	0.6	20	356	16500	2.14	123.2	98.52	1.48
4	**I**	TMA	12	0.6	20	280	11200	2.32	124.2	>99	
5	**I**	TEA	3	0.6	20	722	32800	2.34	149.3	>99	
6	**I**	TEA	6	0.6	20	660	16200	2.21	145.7	>99	
7	**I**	TEA	9	0.6	20	403	13200	2.03	145.5	>99	
8	**I**	TEA	12	0.6	20	360	8900	2.19	132.3	>99	
9	**I**	TEA	9	0.6	30	421	9600	2.07	141.3	>99	
10	**I**	TEA	9	0.6	40	443	7900	2.05	137.8	>99	
11	**I**	TEA	9	0.6	60	541	3900	1.98	112.3	92.12	7.88
12	**II**	TEA	3	0.6	20	533	72000	2.12		15.03	84.97
13	**II**	TEA	3	0.6	40	511	14000	2.30		36.12	63.88

[a] Polymerization conditions: 50 mL of toluene; 4 μmole of zirconium catalyst; 2 mmol of MAO; reaction time = 2 h. [b] Catalyst **I**: $Me_2C(Cp)(Flu)ZrCl_2$. Catalyst **II**: $Me_2Si(Cp)(Flu)ZrCl_2$. [c] TMA = trimethylaluminum; TEA = triethylaluminum. [d] Catalytic activity = kg of polymer/(mole of catalyst-hour). [e] M_n (number-average molecular weight), M_w (weight-average molecular weight), and PDI (polydispersity, M_w/M_n) were determined by high temperature GPC (solvent 1,2,4-trichlorobenzene; temperature 135 °C.) [f] T_m (melting temperature) was determined by DSC. [g] The end group ratios were determined by 500 MHz ^{1}H NMR analyses (solvent, $CDCl_3$; temperature 60 °C).

between the end-functionalized prepolymer and other polymer blocks. These obstacles have been circumvented recently[26] through the successful preparation of structurally well-defined stereoregular end-functionaized prepolymer by employing stereoregular catalyst to mediate the selective chain transfer reaction during stereospecific polymerization of propylene and by linking the stereoregular end-functionalized prepolymer with the second block by anionic coupling route. However, the anionic coupling route still suffers the following problems. First, because of the low solubility of the end-functionalized stereoregular prepolymers in organic solvents, an excess amount of living anionically polymerized polymers has to be added to ensure high coupling efficiency, and this makes complete removal of the residual homopolymer difficult. Second, the structure of the second block is limited to the polymers that can be prepared by living anionic polymerization.

The utilization of hydroxy-terminated end-functionalized polymer as the precursor of macroinitiator (generated by activation with alkylaluminum) for mediating the BCP preparation via controlled ring-opening polymerization of cyclic esters[27] has drawn our attention, as it affords the precise structural controls (of block lengths and molecular weight distribution) for the second block and facilitates the connection of the stereoregular block with a wide variety of polymers. However, employing this synthetic route for preparing stereoregular BCPs requires the synthesis of structurally uniform stereoregular end-functionalized prepolymer[28] carrying a terminal hydroxyl end group.[26b] We have demonstrated recently that the hydroxyl-terminated isotactic polyprolyene can be exclusively generated via inducing selective chain transfer to triethylaluminum (TEA) during polymerization of propylene in the presence of isospecific metallocene catalysts. In this study, we further demonstrate that hydroxy-terminated sPP (OH-capped sPP) can also be selectively produced by conducting propylene polymerization in the presence of syndiospecific metallocene catalysts using TEA as the chain transfer agent. Subsequently, the aluminum alkoxide end-capped sPP macroinitiator can be *in situ* generated (by treating the OH-capped sPP with TEA) and used in mediating the controlled ring-opening copolymerization of ε-caprolactone and DL-lactide for the successful preparations of sPP-*b*-polycaprolactone (sPP-*b*-PCL) and sPP-*b*-polylactide (sPP-*b*-PLA), respectively. The crystallization behavior and morphologies in the melt and crystalline state of these BCPs were also investigated, where sPP-*b*-PCL is a crystalline−crystalline system with both sPP and PCL blocks being crystallizable, whereas sPP-*b*-PLA is a crystalline−amorphous diblock copolymer. The resultant stereoregular BCPs are capable of self-assembling into long-range ordered nanostructures as evidenced by small-angle X-ray scattering (SAXS) analyses.

Experimental Section

General Procedure. All reactions and manipulations were conducted under a nitrogen atmosphere using the standard Schlenk line or drybox techniques. Solvents and common reagents were commercially obtained and were used either as received or purified by distillation with sodium/benzophenone. Propylene (purity >99.9%) and oxygen (purity >99%) were obtained from Matheson and were used as received. The ε-caprolactone (99%) purchased from Aldrich was dried over calcium hydride and distilled under vacuum before use. The DL-lactide (98%) purchased from Aldrich was purified by recrystallization in toluene and dried under vacuum before use. $Me_2C(Cp)(Flu)ZrCl_2$ (**I**)[29] and $Me_2Si(Cp)(Flu)ZrCl_2$ (**II**)[30] were synthesized using the method described in the literature. Trimethylaluminum (TMA, 2 M in hexane) and triethylaluminum (TEA, 1 M in hexane) were purchased from Aldrich and were used as received. Methylaluminoxane (MAO, 14% in toluene), purchased from Albemarle, was dried under vacuum to remove residual TMA.[31] The resulting TMA-free MAO was diluted in toluene to the desired concentration before use.

Preparations of OH-Capped sPP. Representative experiment (for entry 10 of Table 1): A 250 mL stainless steel reactor, equipped with a magnetic stirrer, was allowed to dry at 80 °C under vacuum. After refilled with nitrogen, the reactor was allowed to maintain at 40 °C and then charged sequentially with 50 mL of toluene, 2.0 mmol of MAO, and 4.0 μmol of $Me_2C(Cp)(Flu)ZrCl_2$. After the reaction mixture was allowed to stir at 40 °C for 5 min, the reactor was charged with 9.0 mmol of TEA and then with propylene (0.6 bar) to initiate the polymerization reaction. Polymerization was conducted at 40 °C for 2 h, after which the propylene was discharged from the reactor. The polymer solution was then treated with oxygen at a flow rate of 12 mL/min for 1 h. After that, the solution was slowly cooled to room temperature and was then charged with H_2O_2 (4 mL, 30% in H_2O). After stirring the solution at room temperature for 30 min, the solution was treated with excess methanol (ca. 40 mL), which led to the deposition of the OH-capped sPP as a white precipitate. The resulting polymer was isolated after filtration and dried under vacuum to provide 2.30 g of OH-capped sPP. M_n = 7900, M_w/M_n = 2.05 by GPC (in 1,2,4-trichlorobenzene at 135 °C).

Fractionation of OH-Capped sPP.[32,25] On a vacuum line, 2.30 g of OH-capped sPP (M_n = 7900, M_w/M_n = 2.05, entry 10 of Table 1) was placed in a Soxhlet extractor and was allowed to undergo the first stage of fractionation by Soxhlet extraction in boiling acetone (80 mL) for 24 h. The resulting acetone solution was collected and was allowed to concentrate under vacuum to 10 mL. The resulting solution was then charged with excess methanol

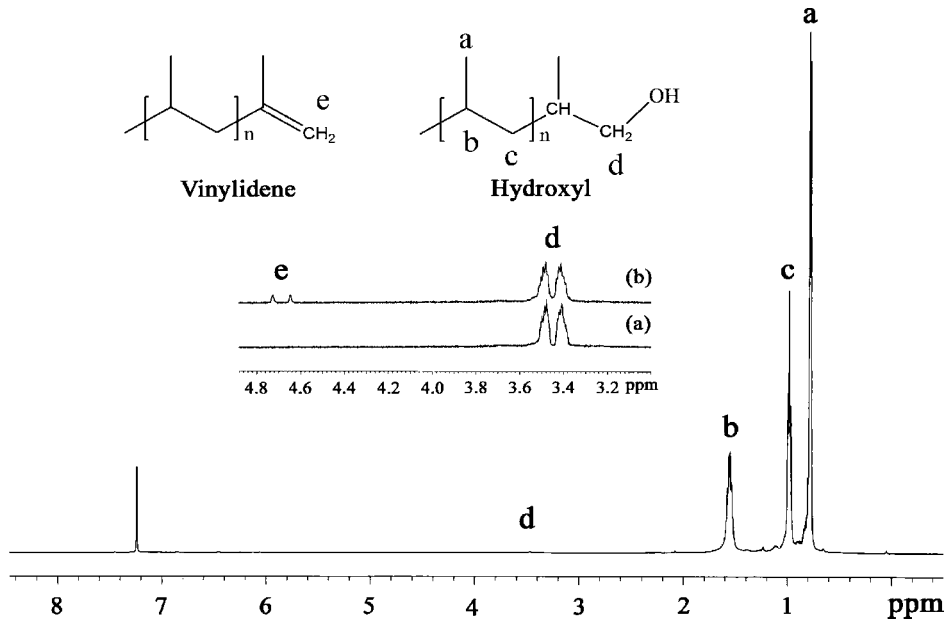

Figure 1. Expanded ^{1}H NMR (500 MHz) region of various sPP samples: (a) M_n = 16200 g/mol, M_w/M_n = 2.21 (run 6 of Table 1); (b) M_n = 20100 g/mol, M_w/M_n = 2.11 (entry 2 of Table 1) (solvent, $CDCl_3$; temperature 60 °C).

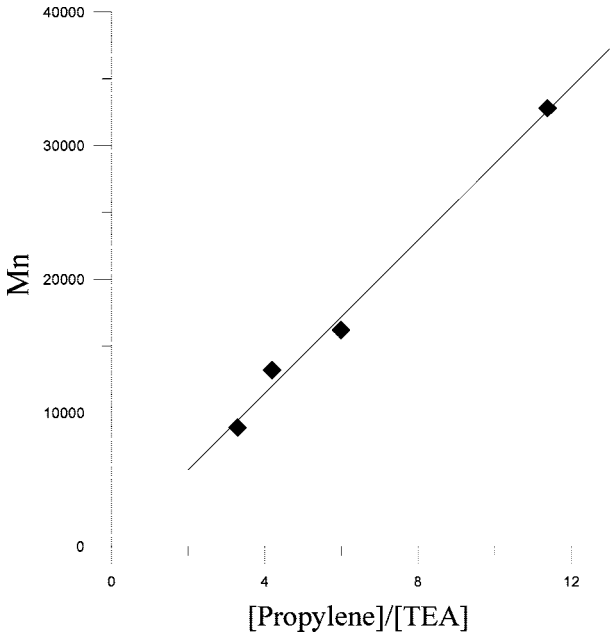

Figure 2. The plot of number average molecular weight (M_n) of OH-capped sPP vs the mole ratios of [propylene]/[TEA] (entries 5−8 of Table 1).

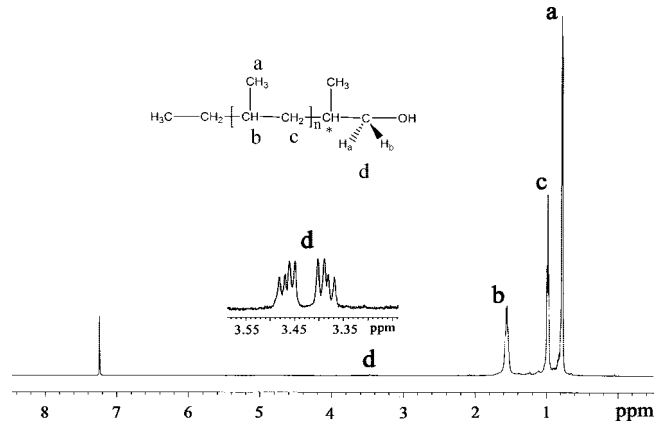

Figure 3. ^{1}H NMR spectra (500 MHz) of the OH-capped sPP (M_n = 7900 g/mol, M_w/M_n = 2.05; entry 10 of Table 1) (solvent, $CDCl_3$; temperature 60 °C).

(ca. 20 mL), which resulted in the deposition of the lower molecular weight, acetone-soluble OH-capped sPP as a white precipitate. The resulting acetone soluble polymer was isolated by filtration and dried under vacuum to provide 0.41 g of OH-capped sPP [M_n = 2430, M_w/M_n = 1.49 by GPC (in 1,2,4-trichlorobenzene at 135 °C); sydiotacticity (*rrrr*) = 74.45%[33] by ^{13}C NMR (solvent $CDCl_3$; temperature 60 °C)].

The acetone insoluble sPP polymer (ca. 1.90 g) was allowed to undergo the second stage of fractionation by Soxhlet extraction in boiling THF for 24 h. The resulting THF solution was collected and was allowed to concentrate under vacuum to 10 mL. The resulting solution was then charged with excess methanol (ca. 25 mL), which in turn resulted in the deposition of the THF soluble OH-capped sPP as a white precipitate. The resulting THF soluble polymer was isolated by filtration and dried under vacuum to provide 0.55 g of OH-capped sPP [M_n = 7350, M_w/M_n = 1.51 by GPC (in 1,2,4-trichlorobenzene at 135 °C); sydiotacticity (*rrrr*) = 79%[33] by ^{13}C NMR (solvent $CDCl_3$; temperature 60 °C)].

Preparation of sPP-*b*-PCL. In a drybox, a 200 mL Schlenk flask equipped with a magnetic stirrer was charged sequentially with 0.25 g (0.10 mmol) of the acetone soluble OH-capped sPP (M_n = 2430, M_w/M_n = 1.49), with 50 mL of toluene and then with 0.11 mmol of TEA. The resulting solution was allowed to stir for 12 h to allow for macroinitiator formation. Then, ε-caprolactone (1.62 g, 11.2 mmol) was added to the flask. The reaction vessel was capped and removed from the drybox. It was then immersed in a 70 °C oil bath and was allowed to undergo the polymerization reaction at 70 °C for 12 h. After that, the reaction was terminated with acidic methanol. The resulting solution was allowed to concentrate to 15 mL by removing volatiles under vacuum. The resulting polymer solution was then charged with excess methanol (ca. 20 mL), and this led to the deposition of the reaction product as an off-white precipitate. The resulting precipitate was isolated by filtration and was allowed to undergo Soxhlet extraction with boiling cyclohexane to remove the residual sPP. The resulting sPP-*b*-PCL was dried under vacuum for 24 h to provide 1.12 g of sPP-*b*-PCL [M_n = 12300, M_w/M_n = 1.14, determined by high-temperature GPC (in 1,2,4-trichlorobenzene at 135 °C); the conversion of ε-caprolactone was 53.7% based on isolation yield].

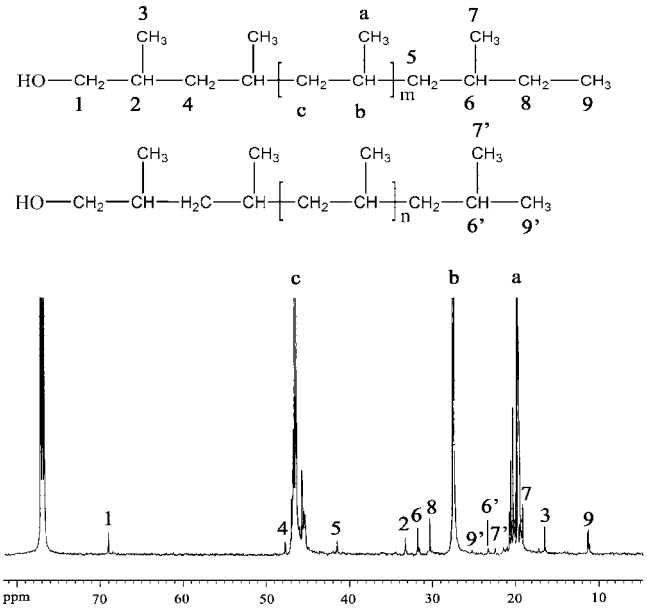

Figure 4. ^{13}C NMR (125 MHz) spectra of the OH-capped sPP (M_n = 7900 g/mol, M_w/M_n = 2.05; entry 10 of Table 1) (solvent, $CDCl_3$; temperature 60 °C).

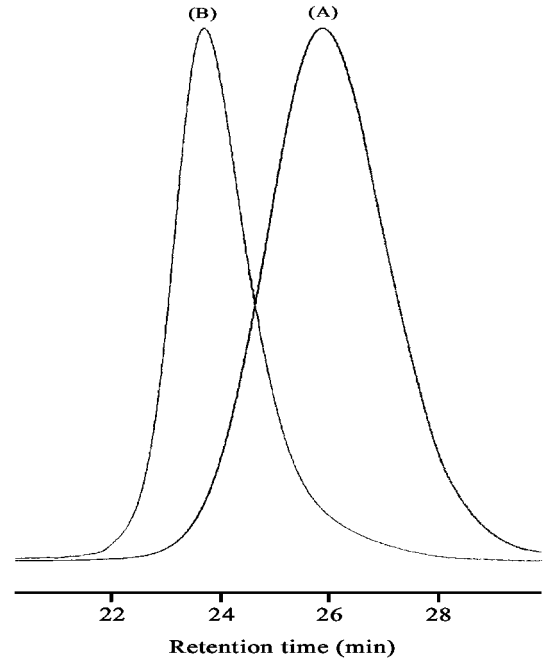

Figure 5. GPC curve comparison between (A) OH-capped sPP (M_n = 2430 g/mol, M_w/M_n = 1.49), (B) sPP-*b*-PCL (M_n = 12300 g/mol, M_w/M_n = 1.14) (in 1,2,4-trichlorobenzene, at 135 °C).

Preparation of sPP-*b*-PLA. In a drybox, a 200 mL Schlenk flask equipped with a magnetic stirrer was charged sequentially with 0.25 g (0.034 mmol) of the THF soluble OH-capped sPP (M_n = 7350, M_w/M_n = 1.51), with 50 mL of toluene and then with 0.035 mmol of TEA. The resulting solution was allowed to stir for 12 h to allow for macroinitiator formation. Then, DL-lactide (0.16 g, 1.1 mmol) was added to the flask. The reaction vessel was capped and removed from the drybox. It was then immersed in a 90 °C oil bath and was allowed to undergo the polymerization reaction at 90 °C for 24 h. After that the reaction was terminated with acidic methanol. The resulting solution was allowed to concentrate to 15 mL by removing volatiles under vacuum. The resulting polymer solution was then charged with excess methanol (ca. 20 mL), and this led to the deposition of the reaction product as an off-white precipitate. The resulting precipitate was isolated by filtration and was allowed to undergo Soxhlet extraction with boiling cyclohexane to remove the residual sPP. The resulting sPP-*b*-PLA was dried under vacuum for 24 h to provide 0.35 g of sPP-*b*-PLA [M_n = 10800, M_w/M_n = 1.34, determined by high-temperature GPC (in 1,2,4-trichlorobenzene at 135 °C); the conversion of DL-lactide was 62.5% based on isolation yield].

Polymer Analysis. Molecular weight and MWD (M_w/M_n) were determined through high-temperature gel permeation chromatography (Waters 150-CALAC/GPC) with a refractive index (RI) detector and a set of U-Styragel HT columns of 10^6, 10^5, 10^4, and 10^3 pore sizes in series. The measurements were taken at 135 °C

Scheme 1

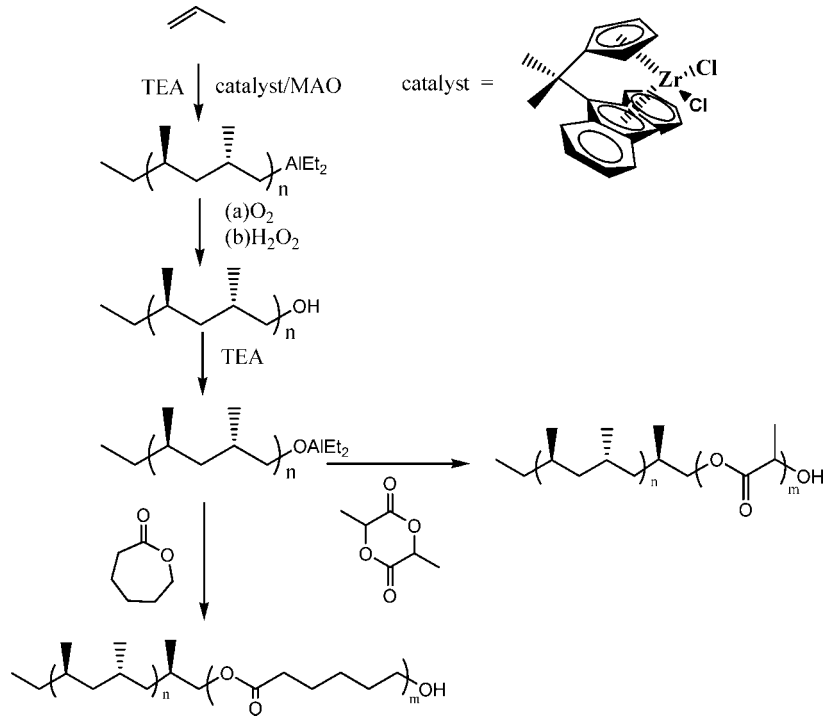

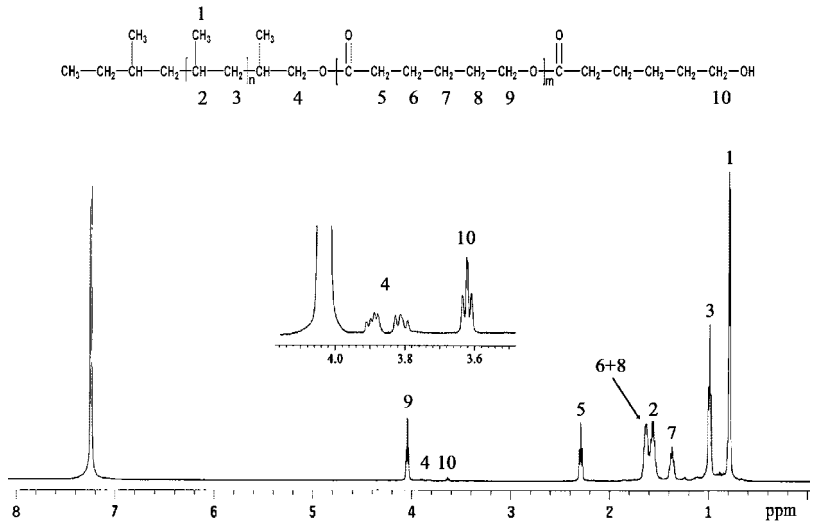

Figure 6. ^{1}H (500 MHz) NMR spectra of the sPP-*b*-PCL (M_n = 12300 g/mol, M_w/M_n = 1.14) prepared form OH-capped sPP (M_n = 2430 g/mol, M_w/M_n = 1.49) (solvent, $CDCl_3$; temperature, 60 °C).

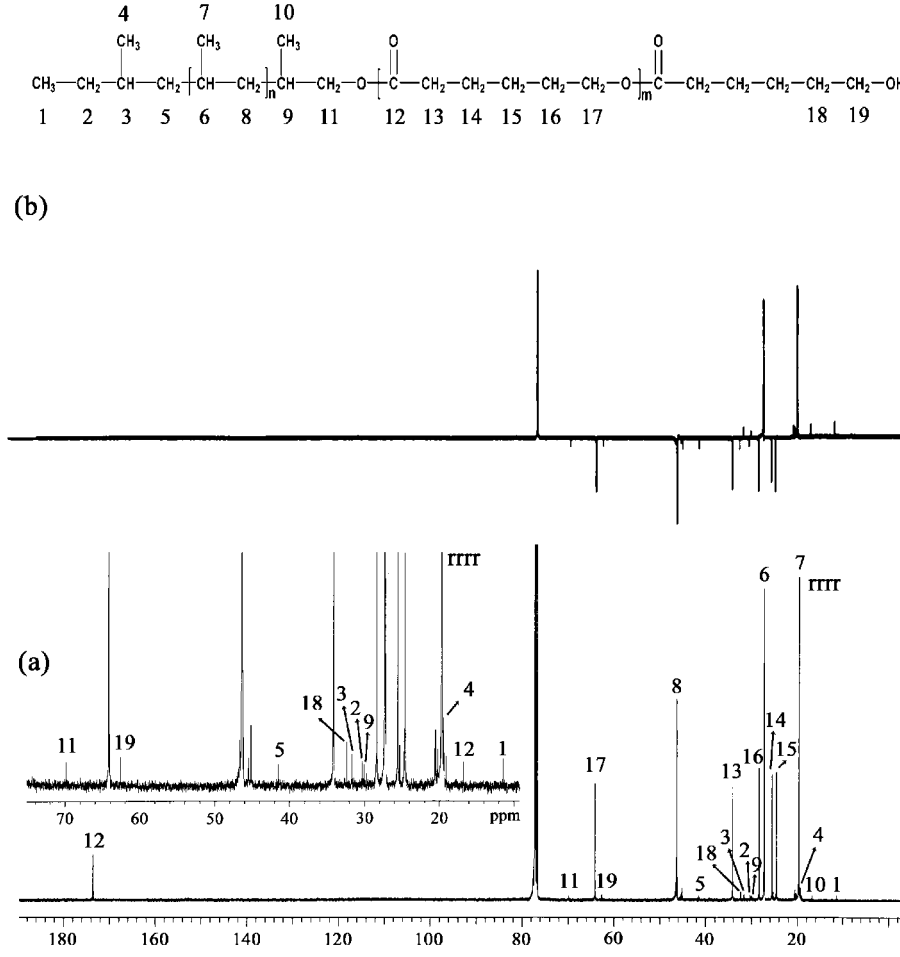

Figure 7. (a) ^{13}C and (b) ^{13}C (DEPT 135) NMR (125 MHz) spectra of the sPP-*b*-PCL (M_n = 12300 g/mol, M_w/M_n = 1.14) prepared from OH-capped sPP (M_n = 2430 g/mol, M_w/M_n = 1.49) (solvent, $CDCl_3$; temperature, 60 °C).

using 1,2,4-trichlorobenzene as solvent. PS samples with narrow MWDs were used as the standards for calibration. The standards were in the range of absolute molecular weight, which is from 980 to 2110000; the *R* square of the ideal calibrated line was limited to up to 0.999.

The ^{1}H (500 MHz) and ^{13}C NMR (500 MHz) spectra were recorded on a Bruker AV-500 NMR spectrometer. The sPP-based samples were dissolved into $CDCl_3$ or benzene-d_6 as solvents. The recorded temperature was at 60 °C.

Bulk Sample Preparation. The bulk samples of sPP-*b*-PCL and sPP-*b*-PLA were prepared by dissolving the BCPs in tetrahydrofuran (THF) at 60 °C. The concentration of the polymers in the solution was 5 wt %. The samples were subsequently cast onto the Petri dishes followed by a slow evaporation of the solvent at 30 °C for

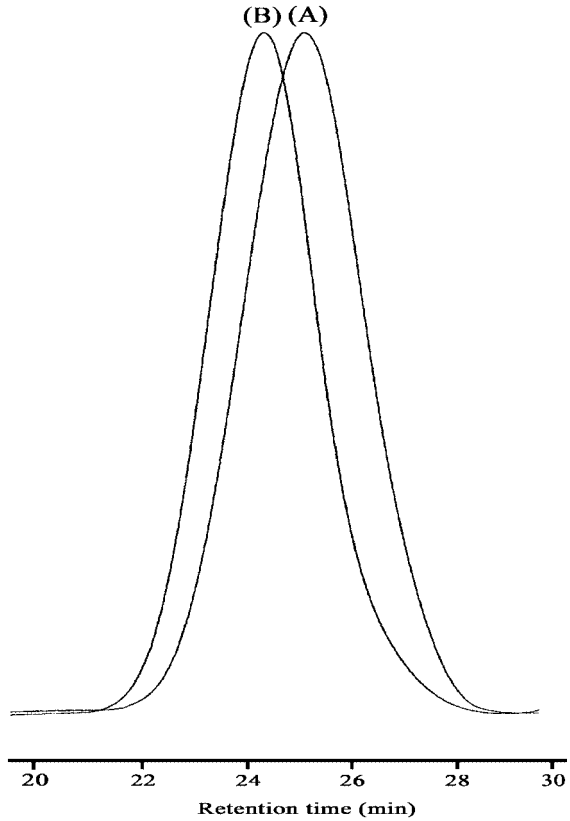

Figure 8. GPC curve comparison between (A) OH-capped sPP (M_n = 7350 g/mol, M_w/M_n = 1.51) and (B) sPP-*b*-PLA (M_n = 10800 g/mol, M_w/M_n = 1.34) (in 1,2,4-trichlorobenzene, at 135 °C).

two days. The samples were further dried in vacuum at 60 °C for 2 h and then at room temperature for four days for complete solvent removal. The resultant films of the BCPs were studied by SAXS and differential scanning calorimetry (DSC).

Differential Scanning Calorimetry (DSC) Measurement. The crystallization and melting behavior of sPP-*b*-PCL and sPP-*b*-PLA for nonisothermal condition were studied by a TA DSC-2010 instrument. Samples were encapsulated in aluminum pans, and their mass was approximately 5 mg. The calibration was performed with indium and all tests were run employing ultra pure nitrogen as purge gas. In the standard DSC experiments, the samples were first heated to 200 °C, which was above the melting points of both sPP and PCL blocks, and kept at that temperature for 5 min to erase thermal history. Then a cooling scan at 10 °C/min was conducted down to −40 °C, followed by a subsequent heating run performed also at 10 °C/min.

Small Angle X-ray Scattering (SAXS) Measurement. Morphologies of the BCPs in the melt and crystalline state were characterized by a Bruker Nanostar SAXS instrument. The X-ray source, a 1.3 kW X-ray generator (NANOSTAR, Bruker Co, Ltd.) equipped with a Cu tube, was operated at 40 kV and 35 mA. The scattering intensity was detected by a two-dimensional position-sensitive detector (Bruker AXS) with 512 × 512 channels. The area scattering pattern has been radially averaged to increase the photon counting efficiency compared with the one-dimensional linear detector. The intensity profile was output as the plot of the scattering intensity (I) vs the scattering vector, $q = 4\pi/\lambda \sin(\theta/2)$ (θ = scattering angle). All of the SAXS profiles were corrected for the empty beam scattering, the sensitivity of each pixel of the area detector, and the background arising from thermal diffuse scattering (TDS). The intensity level of TDS was assumed to be a constant over the q range covered in this study, and its magnitude was determined from the slope of the Iq^4 vs q^4 plot at the high-q region ($q > 1.3$ nm^{-1}). SAXS measurements were performed under vacuum to minimize the thermal degradation of the samples.

Results and Discussion

Preparations of Hydroxyl-Capped sPP by Selective Chain Transfer to Alkylaluminums.[25d] The OH-capped sPP was prepared by conducting the syndiospecific propylene polymerization in the presence of different *ansa*-metallocene catalysts [$(Me)_2C(Cp)(Flu)ZrCl_2$ (**I**) and $(Me)_2Si(Cp)(Flu)ZrCl_2$ (**II**)] using TMA or TEA as the chain transfer agents, and this led to the generation of the alkylaluminum-capped sPP as the preliminary product. After the polymerization, the polymer solution was in situ treated with O_2/H_2O_2[34,26b] for converting the aluminum end group to the hydroxyl terminal group to give OH-capped sPP. The resulting polymer solution was then charged with excess methanol, leading to the deposition of sPPs as a white precipitate. ^{1}H and ^{13}C NMR spectra of the sPPs produced under these conditions were evaluated to determine the chain end structures. The results of the polymerization studies are summarized in Table 1.

As shown in Figure 1 (entries 10 and 2 of Table 1), sPPs with two different chain end structures, including hydroxyl and vinylidene end groups, can be generated under these reaction conditions. The hydroxyl end group was produced from the primary insertion propylene unit, which underwent chain transfer to aluminum so as to give aluminum-capped sPP as the preliminary reaction product; subsequently, the in situ oxidation of the resulting aluminum-capped sPP by the method described in the Experimental Section led to the generation of OH-capped sPP. The vinylidene chain end was generated form the primary insertion propylene unit, which, by contrast, underwent β-hydride elimination chain transfer. It should be noted that we are unable to detect any allyl and 2-butenyl end-capped sPPs. Evidently, chain releasing by β-methyl elimination (generating allyl chain end) and by the formation of a secondary insertion propylene unit that underwent subsequent β-hydride elimination transfer (generating 2-butenyl chain end) failed to take place when propylene polymerizations were conducted in the presence of the fluorenyl lignad containing catalysts **I** and **II**. We also found that the ratio of the OH-capped sPP is strongly dependent on the structures of metallocene catalysts as revealed by the comparison results between entries 1−11 and 12−13. Evidently, conducting the propylene polymerization in the presence of the C-bridged catalyst (**I**) provided mainly the hydroxyl terminated sPP; whereas, vinylidene terminated sPP was predominantly generated by conducting the propylene polymerization in the presence of the Si-bridged catalyst (**II**).

The comparison of results between entries 1−4 and entries 5−8 clearly indicates that replacing TMA with TEA reduces the ratio for vinylidene-capped sPP formation and results in the formation of the OH-capped sPP as the only reaction product. These results clearly indicate that TEA has a higher chain transfer rate than TMA when conducting the syndiospecific propylene polymerization in the presence of catalyst **I**. Figure 2 shows the plot of polymer molecular weight versus [propylene]/[TEA] by conducting the propylene polymerization at 20 °C using $(Me)_2C(Cp)(Flu)ZrCl_2$ (**I**) as the catalyst and TEA as the chain transfer agent (entries 5−8). The nearly linear relationship between the molecular weight of sPPs and [propylene]/[TEA] ratio indicates that chain transfer to TEA (rate constant = k_{tr}) compete with the propylene chain propagation reaction. Since the degree of polymerization (X_n) follows the equation $X_n = k_p[\text{propylene}]/k_{tr}[\text{TEA}]$, the plot in Figure 2 provides the calculation of the chain transfer constant (k_{tr}/k_p = 1/68.17) for the generation of OH-capped sPP by the predominant chain transfer to TEA. Noted that a lower chain transfer rate constant was observed in the production of OH-capped sPP comparing with the prior results for the generation of OH-capped iPP.[26b] The lower chain transferring rate in the production of OH-capped sPP could be attributed to the fact that OH-capped

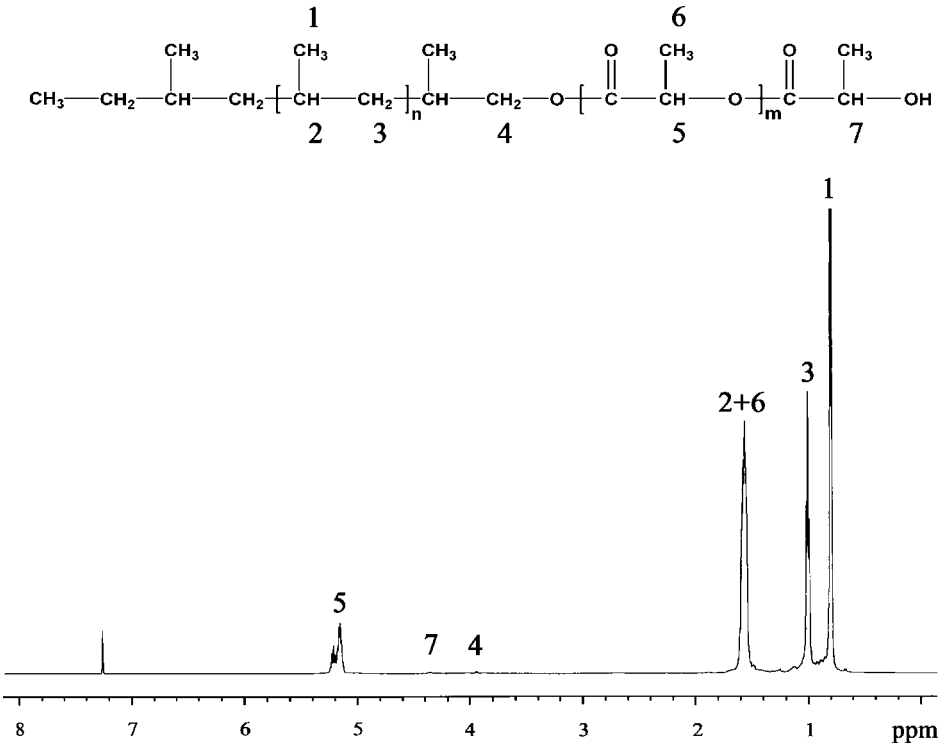

Figure 9. ^{1}H (500 MHz) NMR spectra of the sPP-*b*-PLA (M_n =10800 g/mol, M_w/M_n = 1.34) prepared from OH-capped sPP (M_n = 7350 g/mol, M_w/M_n = 1.51). (solvent, $CDCl_3$; temperature, 60 °C).

sPP was generated by using the bulky fluorenyl containing catalyst (I), which may retard the chain transfer efficiency because of the steric repulsion between the fluorenyl ligand and the chain transfer agent (TEA). Nevertheless, our results first demonstrated that hydroxy-capped sPP can be selectively generated by inducing the selective chain transfer to TEA via conducting the syndiospecific propylene polymerization in the presence of *ansa*-metallocene catalysts.

End Group Analyses. End group analyses provide the detailed structural information for sPPs prepared under the reaction conditions and give direct evidence for the successful preparation of the pure OH-capped sPP. Figure 3 elucidates the ^{1}H NMR spectrum (with an inset of the expanded region and chemical shift assignments) of the OH-capped sPP (M_n = 7900 M_w/M_n = 2.25; entry 10 of Table 1) isolated after the O_2/H_2O_2 treatment. The characteristics of the two sets of doublet of doublets coupling patterns [δ = 3.38 and 3.47 (2 H, dd, $J_{geminal}$ = 10.0 Hz and $J_{vicinal}$ = 6.25 Hz)] correspond to the $-CH(CH_3)-CH_2-OH$ methylene proton resonances situated in a diastereotopic environment. Figure 4 shows the ^{13}C NMR spectrum (with an inset of the chemical shift assignments) of the hydroxy-capped sPP (M_n = 7900 M_w/M_n = 2.05; entry 10 of Table 1). The detailed chemical assignments are based on the structural information revealed in ^{13}C (DEPT 135), two-dimensional ^{1}H and ^{1}H COSY, ^{13}C and ^{1}H HMQC (Supporting Information) NMR spectra, and by comparison with prior NMR analyses of OH-capped iPP[26b] and sPP.[35] These NMR spectra clearly revealed that OH-capped sPP possesses a uniform hydroxyl terminal group for use as the stereoregular end-functionalized prepolymer in the construction of stereoregular BCPs. It is interesting to note that two aliphatic chain ends, namely, isobutyl [$CH_3CH_2CH(CH_3)-$] (approximately 82% based on integration) and isopropyl [$CH_3CH(CH_3)-$] (approximately 18% based on integration), which were generated in the chain initiation steps, can be identified by these ^{13}C NMR analyses (Figure 4). The isobutyl end group was generated in the chain initiation step by primary insertion of propylene to [Zr−Et], which was formed in the chain releasing step by the selective chain transfer to TEA. By contrast, the isopropyl end group was generated by primary insertion of propylene to [Zr−Me], which was formed in the chain releasing step by chain transfer to MAO or to the residual TMA in the MAO solution. The identical chain end structures both in OH-capped sPP and OH-capped iPP[26b] clearly demonstrated that the formation of these OH-capped PPs involves similar chain transfer pathways.

Preparations of Stereoregular Diblock Copolymers of Syndiotactic Polypropylene and Polyesters. As demonstrated from the chain end analysis, the OH-capped sPP contains a uniform hydroxyl end group to be used as the end-functionalized prepolymer for the synthesis of stereoregular BCPs. However, the OH-capped sPP prepolymer prepared form the nonliving coordination polymerization (metallocene) process a broad range of molecular weight distribution and is not suitable for use directly in the post block polymerization reaction for preparations of structurally well-defined stereoregular BCPs. Although it has been demonstrated that BCPs with relatively high polydispersity are still able to self-assemble into ordered morphologies, the broad distribution in chain length would shift the phase boundaries (relative to those of the corresponding monodisperse BCPs) and modify the microdomain size.[36] Because the present study intends to check the consistency of the morphology self-organized by the prepared stereoregular BCPs with that predicted by the classical phase diagram of monodisperse diblock copolymers under the prescribed volume fraction and segregation strength, it is desirable to reduce the polydispersity of the prepared BCPs as well as to have a precise control over the molecular chain length. In this case, the preparation of stereoregular BCPs has to start from an end-functionalized stereoregular prepolymer having a narrow range of MWD.[25] The narrow MWD sample of OH-capped sPP can be obtained by the fractionation of the broad MWD product through extraction processes.[26,32] Thus, fractionation by sequential Soxhlet extractions in acetone and then in THF by methods described in the Experimental Section provided two suitable samples of OH-capped sPPs [M_n = 2430, MWD = 1.49, syndiotacticity (*rrrr*) = 74.45%, isolated from acetone extrac-

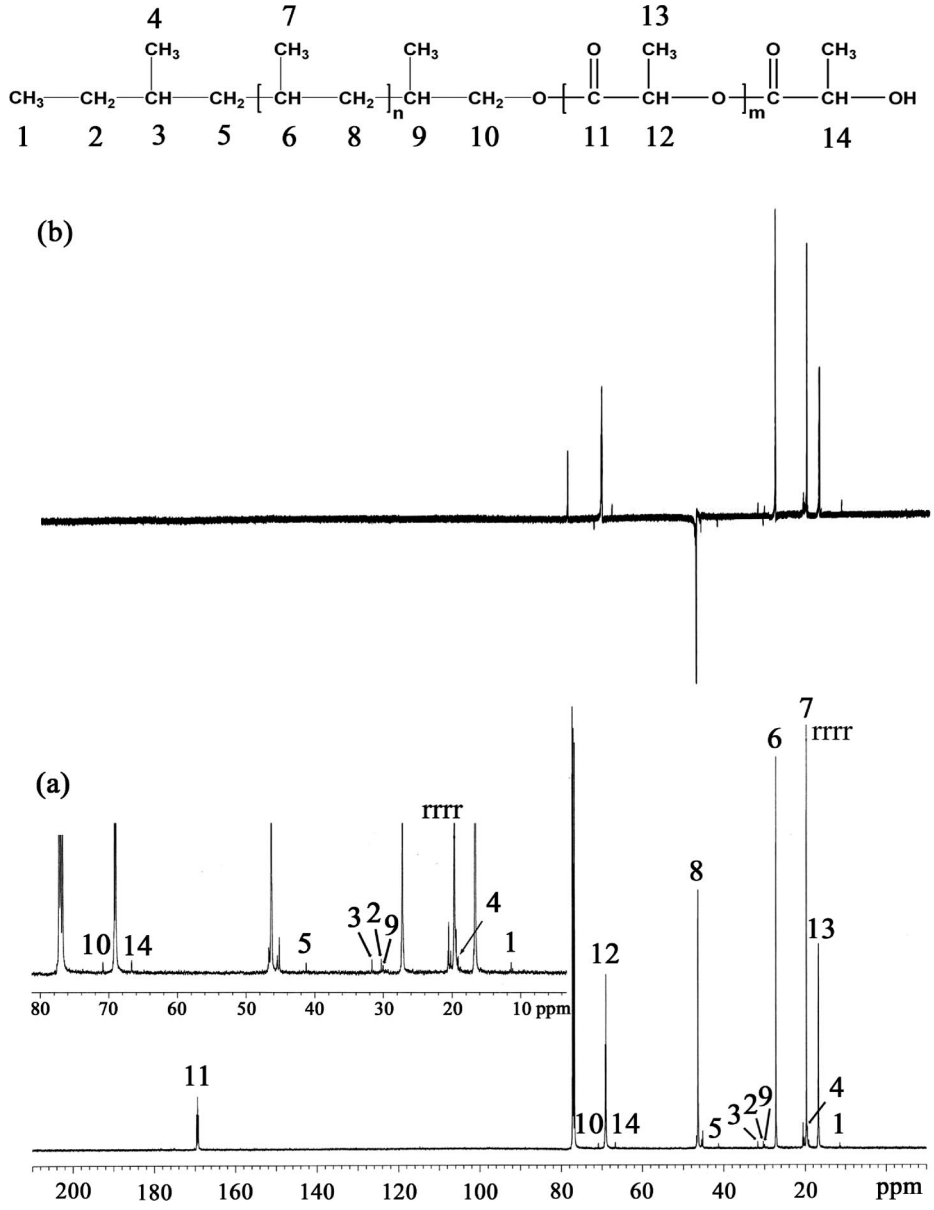

Figure 10. (a) ^{13}C and (b) ^{13}C (DEPT 135) NMR (125 MHz) spectra of the sPP-*b*-PLA-1 (M_n =10800 g/mol, M_w/M_n = 1.34) prepared from OH-capped sPP (M_n = 7350 g/mol, M_w/M_n = 1.51) (solvent, $CDCl_3$; temperature, 60 °C).

Table 2. Molecular Characteristics of the Block Copolymers and Homopolymers

sample	$M_{n,exp}$[a] total	PDI[a]	volume fraction of sPP block[b]
sPP (2430)	2434	1.49	1.0
sPP-*b*-PCL	12347	1.14	0.24
sPP (7300)	7350	1.51	1.0
sPP-*b*-PLA	10783	1.34	0.73

[a] M_n (number-average molecular weight), M_w (weight-average molecular weight), and PDI (polydispersity, M_w/M_n) were determined by high-temperature GPC (solvent,1,2,4-trichlorobenzene; temperature, 135 °C). [b] Calculated from the molecular weights of sPP and PCL blocks.

tion; M_n = 7350, MWD = 1.51, syndiotacticity (*rrrr*) = 79.46%, isolated from THF extraction] for use in the preparation of sPP block containing stereoregular BCPs. As these end-functionalized prepolymers possess the uniform hydroxyl end group, converting the hydroxyl end group to aluminum alkoxide-capped sPP by methods developed by Hillmyer[37] led to the successful generation of the sPP-macroinitiator. Although our prior studies[26] revealed that the preparation of stereoregular BCPs via postpolymerization of the lithiated anionic stereoregular macroinitiator failed to give satisfactory results, the aluminum alkoxide-capped sPP macroinitiator has been demonstrated to be highly effective for mediating the controlled ring-opening block copolymerization of cyclic esters for the production of sPP-*b*-polyester copolymers.

Accordingly, the OH-capped sPP [M_n = 2430, MWD = 1.49, syndiotacticity (*rrrr*) = 74.45%] was treated with an equal molar of TEA that led to the successful formation of the aluminum alkoxide-capped sPP macroinitiator. Subsequently, conducting the controlled ring-opening block copolymerization of the sPP-macroinitiator with ε-caprolactone at 70 °C provides sPP-*b*-PCL with a good ε-caprolactone conversion ratio and high BCP yield. The detailed synthetic routes for the preparation of sPP-*b*-PCL are illustrated in Scheme 1. Figure 5 compares the GPC elusion curves of OH-capped sPP with the sPP-*b*-PCL (M_n = 12300, MWD = 1.14). Figure 6 and Figure 7 show the ^1H NMR and ^{13}C and ^{13}C (DEPT 135) NMR spectra (with insets of expanded region and the chemical shift assignments) of the sPP-*b*-PCL. The presence of a single junction chemical structure (sPP−*CH*(*CH*$_3$)−*CH*$_2$−O−PCL) as characterized by comparing the relative intensities between the sPP chain end, PCL chain end and the junction structure shown in these NMR spectra

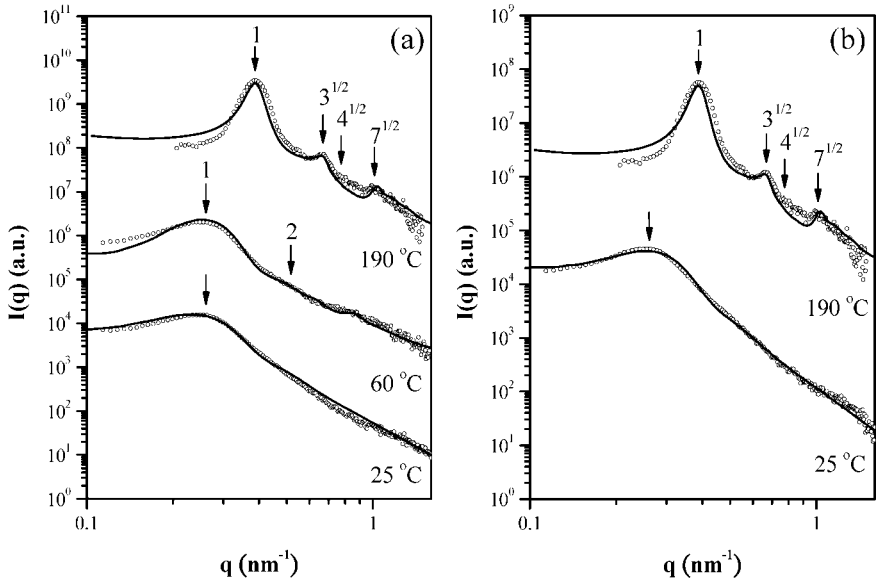

Figure 11. (a) SAXS profiles of sPP-*b*-PCL (M_n = 12300 g/mol, M_w/M_n = 1.14) subjecting to a two-stage crystallization. The system was cooled from 190 to 60 °C to allow sPP crystallization for 30 min followed by cooling to 25 °C to induce PCL crystallization. (b) SAXS profiles of sPP-*b*-PCL subjecting to one-stage crystallization. The system was cooled directly from 190 to 25 °C to allow the crystallizations of both sPP and PCL blocks. The solid curves represent the fits by the paracrystalline model of hexagonally packed cylinders (for the profile collected at 190 °C) or the paracrystalline model of lamellar structure (for the profile collected at 60 and 25 °C).

Table 3. Structural Parameters Obtained from the Fittings of the Experimental SAXS Profiles by the Paracrystalline Model of Hexagonally-Packed Cylinders (for the BCPs in the Melt State) or the Paracrystalline Model of Lamellar Structure (for the BCPs in the Crystalline State)

	sPP-*b*-PCL			sPP-*b*-PLA		
parameter	T = 190 °C	T = 60 °C (190 ° → 60 °C)	T = 25 °C (190 °C → 60 ° → 25 °C)	T = 25 °C (190 °C → 25 °C)	T = 190 °C	T = 80 °C (190 °C → 80 °C)
D (nm)[a]	18.75	21.33	20.80	19.13	20.50	19.26
grain size (nm)	75.10	50.27	40.10	38.49	110.20	40.20
g[b]	0.066	0.093	0.150	0.183	0.063	0.163
R (nm)[c]	4.95	62.47	80.42	89.47	5.58	88.45
σ_R[d]	0.14	0.13	0.22	0.22	0.19	0.22
L (nm)[e]	100.0	6.13	6.02	5.45	100.0	5.74
σ_L[f]	0.15	0.25	0.34	0.33	0.15	0.50

[a] Interdomain distance [b] Ratio of the mean displacement of the lattice points to the interdomain distance [c] Average radius of the cylindrical microdomains (in the melt state) or the lamellar microdomains (in the crystalline state) [d] Polydispersity of the radius given by the ratio of the standard deviation of the distribution to the average radius [e] Average length of the cylindrical microdomains (in the melt state) or the average thickness of the lamellar microdomains (in the crystalline state) [f] Polydispersity of the length or thickness given by the ratio of the standard deviation of the distribution to the average length or thickness.

clearly indicates the successful preparation of the pure sPP-*b*-PCL and the absence of homopolymers.

It is worth noting that the sPP-based aluminum alkoxide macroinitiator can also be used for the controlled ring-opening block copolymerization of lactide, resulting in the generation of the structurally well-defined sPP-*b*-PLA for self-assembly studies. Accordingly, the OH-capped sPP [M_n = 7350, MWD = 1.51, syndiotacticity (*rrrr*) = 79.46%] was treated with an equal molar of TEA for providing the aluminum alkoxide-capped sPP macroinitiator. The resulting sPP macroinitiator was allowed to undergo the controlled ring-opening block copolymerization of DL-lactide at 90 °C to give sPP-*b*-PLA with a high DL-lactide conversion ratio and high BCP yield. The detailed synthetic routes for the preparation of sPP-*b*-PLA are elucidated in Scheme 1. Figure 8 compares the GPC elusion curves of OH-capped sPP with the sPP-*b*-PLA (M_n = 10800, MWD = 1.34). Figure 9 and Figure 10 show the ^{1}H NMR and ^{13}C and ^{13}C (DEPT 135) NMR spectra (with insets of expanded region and the chemical shift assignments) of the sPP-*b*-PLA. The presence of the single junction geometry (sPP−*CH*(*CH*$_3$)−*CH*$_2$−O−PLA) as characterized by comparing the relative intensities between the sPP chain end, PLA chain end and the junction structure shown in these NMR spectra clearly reveals the successful preparation of the pure sPP-*b*-PLA and the absence of homopolymers.

Microphase-Separated Morphology of Stereoregular BCPs. Two stereoregular BCPs, sPP-*b*-PCL and sPP-*b*-PLA, have been prepared in this study. The molecular characteristics of the copolymers are summarized in Table 2. sPP-*b*-PCL is a crystalline−crystalline system with both sPP and PCL blocks being crystallizable, whereas sPP-*b*-PLA is a crystalline−amorphous diblock copolymer. The state of segregation of these two copolymers can be assessed by their χN values. The Flory−Huggins interaction parameter χ was estimated from the equation $V_u(\delta_{sPP} - \delta_{polyester})^2/RT$, where the reference volume V_u was chosen as the molar segmental volume and the solubility parameters of sPP, PCL and PLA were approximately 15.60,[38] 19.20,[39] and 20.02[40] (J/cm^3)$^{1/2}$, respectively. The values of χN at 190 °C thus calculated were 45.6 and 73.2 for sPP-*b*-PCL and sPP-*b*-PLA, respectively. Therefore, both systems should exhibit the intermediate segregation strength ($10.5 < \chi N < 100$) according to the mean-field theory.[41]

Figure 11a shows the SAXS profiles of sPP-*b*-PCL collected in situ at different temperatures in a cooling cycle. At 190 °C where both sPP and PCL blocks were in the melt state (T_m^{PCL}

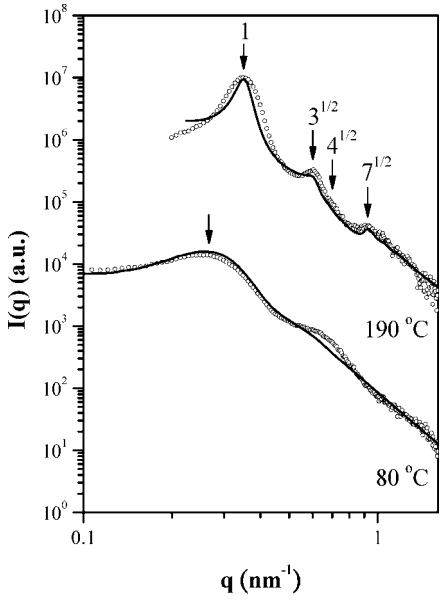

Figure 12. SAXS profiles of sPP-*b*-PLA (M_n = 10800 g/mol, M_w/M_n = 1.34) subjecting to the crystallization process at 80 °C. The system was cooled from 190 to 80 °C to allow sPP crystallization for 30 min followed by data acquisition. The solid curves represent the fits by the paracrystalline model of hexagonally packed cylinders (for the profile collected at 190 °C) or the paracrystalline model of lamellar structure (for the profile collected at 80 °C).

< T_m^{sPP} < 190 °C < T_{ODT}), the SAXS profile showed multiple scattering peaks with the position ratio of $1:3^{1/2}:4^{1/2}:7^{1/2}$. This indicated that sPP-*b*-PCL exhibited a hexagonally packed cylinder morphology, where the minority sPP blocks formed the cylindrical microdomains dispersed in the PCL matrix. This morphological pattern was consistent with that predicted by the classical mean-field phase diagrams[41] under the given volume fraction and segregation strength. The solid curve superposing on the SAXS profile represents the fit using the paracrystalline model of hexagonally packed cylinders considering the polydispersities of the cylinder radius and length, the domain (grain) size of the lattice and the lattice distortion by thermal fluctuations.[42] The interdomain distance (D) and the average radius (R) of the sPP cylinder derived from the fit were 18.7 and 4.95 nm, respectively (cf. Table 3). The volume fraction of the sPP cylinder deduced from the values of R and D was 0.25, which agreed well with the value (0.24) prescribed by the molecular weights of sPP and PCL blocks.

When the sPP-*b*-PCL was cooled to 60 °C (T_m^{PCL} < 60 °C < T_m^{sPP} < T_{ODT}) and kept at this temperature for 30 min, sPP crystallization took place in the cylindrical microdomains surrounded by the soft PCL phase. In this case, the BCP was a crystalline−amorphous system where the crystallization process of the sPP block could perturb the melt mesophase. It can be seen from Figure 11a that the primary peak in the corresponding SAXS profile shifted to lower q and became broader (comparing to that observed at 190 °C), indicating that the morphological perturbation did take place. A vague second-order peak could be identified near 0.50 nm^{-1}, implying that the crystallization of sPP block disrupted the melt structure and transformed it into a crystalline lamellar morphology. This type of breakout crystallization has been reported for crystalline−amorphous diblock copolymers with minor crystalline component.[5b,43,44] The solid curve superposing on the SAXS profile represents the fit using the paracrystalline model of one-dimensionally stacked lamellar microdomains. The values of the structure parameters obtained from the fit are listed in Table 3. It can be seen that the lamellar model yielded satisfactory fit to the experimental data; in this case, the driving force of crystallization overwhelmed that stabilizing the melt mesophase due to the relatively weak segregation strength of the copolymer, such that the crystallization process broke out the cylindrical domains to form large-scale crystalline lamellar domains.

As the system was further cooled to 25 °C at which the crystallization of PCL block could occur, the SAXS peak became even broader, indicating that PCL crystallites formed between the sPP crystalline lamellae and such a crystallization process reduced the coherent order of lamellar stacking. This was supported by the larger value of the g factor (defined as ratio of the mean displacement of the lattice points to the interdomain distance) derived from the fit of the paracrystalline model for lamellar structure compared with that obtained for the copolymer at 80 °C (cf. Table 3).

Figure 11b shows the SAXS profile of sPP-*b*-PCL collected by direct quenching the diblock from 190 to 25 °C. Upon quenching to 25 °C for 30 min, the crystallizations of both sPP and PCL blocks took place and competed with each other. Nevertheless, the SAXS profile after the crystallization was almost identical with that collected at 25 °C for the sample subjecting to the "two-stage crystallization" shown in Figure 11a, as manifested by the similar fitting parameters for the paracrystalline model (cf. Table 3). This implied that upon quenching to 25 °C the crystallization of sPP blocks occurred first (presumably due to the much larger degree of undercooling) and it broke out the pre-existing mesophase to form the lamellar morphology. The crystallization of PCL blocks then set in within the hard-confined space established by the sPP component.

In contrast to the sPP-*b*-PCL in which the sPP block formed the discrete cylindrical microdomains, the sPP block in the sPP-*b*-PLA synthesized here (f_{sPP} = 0.73) formed the matrix phase. Figure 12 shows the SAXS profiles of sPP-*b*-PLA collected at 190 and 80 °C (cooled from 190 °C). At 190 °C, where both blocks were in the melt state, the scattering pattern was characterized by a series of peaks showing the position ratio of $1:3^{1/2}:4^{1/2}:7^{1/2}$, indicating that the PLA block formed the cylindrical microdomains packed in a hexagonal lattice. The observed melt mesophase again agreed with that predicted by the classical phase diagrams.[41] The fit using the paracrystalline model of hexagonally packed cylinders yielded the interdomain distance and the average radius of the PLA cylinder of 20.5 and 5.6 nm, respectively (cf. Table 3). The volume fraction of the sPP cylinder deduced from the values of R and D was 0.27, which agreed well with the value (0.27) prescribed by the molecular weights of sPP and PLA blocks.

As the sPP-*b*-PLA was cooled to 80 °C and kept at this temperature for 30 min, sPP was able to crystallize in the regions between the rubbery PLA cylinders. The SAXS profile collected after the crystallization displayed a primary peak (locating at significantly lower q than that observed at 190 °C) along with a broad shoulder at ca. 0.65 nm^{-1}. The scattering pattern could also be fitted fairly well by the paracrystalline model for lamellar structure with the parameters listed in Table 3. This indicated that the hexagonally packed cylinder structure in the melt state was disrupted by sPP crystallization and transformed into a lamellar morphology with the interlamellar distance of 19.3 nm. The breakout process induced by sPP crystallization was again attributable to the relatively weak segregation length in sPP-*b*-PLA.

The crystallization kinetics and the melting behavior of the two sPP-based BCPs have also been assessed by DSC. Figure 13a and (b) show the DSC cooling and subsequent heating scans of two sPP homopolymer precursors (for the BCP preparation) and the sPP-containing BCPs. The cooling scans revealed an exotherm associated with the crystallization of sPP upon the cooling, while the heating scans taken immediately showed the

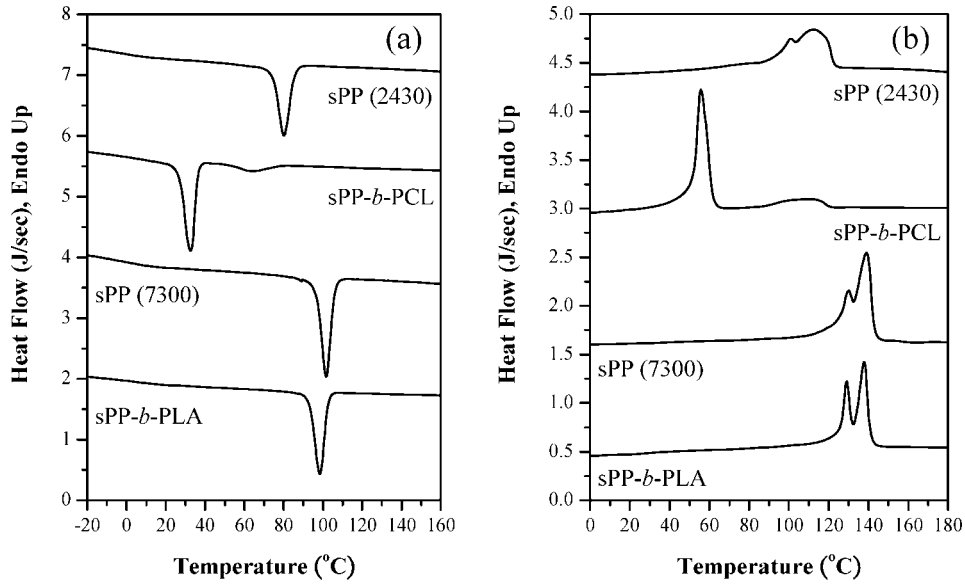

Figure 13. DSC (a) cooling and (b) subsequent heating scans of two sPP homopolymer precursors (for the BCP preparation) and the sPP-containing BCPs. Both scans were conducted at the cooling or heating rate of 10 °C/min.

Table 4. Thermal Properties of sPP Homopolymers and sPP-*b*-Polyesters Obtained from the DSC Thermograms Presented in Figure 13

	sPP				PCL			
sample	T_c, °C	T_m, °C	ΔH_c, J/g	ΔH_m, J/g	T_c, °C	T_m, °C	ΔH_c, J/g	ΔH_m, J/g
sPP(2430)	80.2	101.0, 112.3	59.6	60.6				
sPP-*b*-PCL (12300)	64.2	110.1	11.1	13.4	32.7	55.4	64.7	65.1
sPP(7300)	102.1	131.5, 140.1	82.7	86.75				
sPP-*b*-PLA (10800)	98.3	129.2, 138.0	53.75	55.44				

melting endotherms of the sPP crystals. The measured thermal properties are listed in Table 4.

For all samples under study, two melting peaks attributable to different thermal stabilities of the crystals were observed in Figure 13b. It had been reported that sPP[45,46] may display double melting peaks, especially for the samples with lower syndiotacticity.[45,47,48] The two melting peaks not only showed heating- and cooling-rate dependence but were also affected by crystallization temperature.[49−52] Several models have been proposed to explain the multimelting behavior. Simultaneous melting−recrystallization−remelting[53−55] and the dual-lamellar population models[56−59] were the two main models. The double melting behavior of both sPP and the BCPs could be successfully explained by the mechanism proposed by Cheng et al.[52] that the lower melting crystals may undergo reorganization and melt-recrystallization to form the higher-melting crystals. During this transformation, doubling of the crystal unit cell along the *b* axis with an antichiral packing of the chain molecules (Cell III)[60−62] occurred. In this case, the phenomenon of double melting peaks was associated with the changes of chain packing in the crystal structure toward the full antichiral packing and doubling of the unit cell. This type of unit cell in sPP caused the higher melting peak to contribute to a large part of the enthalpy of melting. On the other hand, a small portion of the lower melting peak might be attributed to the unit cell of intermolecular packing disorder along the *b*-axis in sPP crystals.[60] Indeed, the selection of the opposite handedness in chain molecules should be dominated by the competition between the molecular motion and the crystallization rate, and should be both molecular-weight and temperature dependent. In the case of sPP-*b*-PLA, the increase of the enthalpy of melting of the lower melting peak might be due to the tethering of the sPP blocks to the microdomain interface, which increased the population of random chain packing unit cell in sPP crystal due to decreased molecular motion.

For sPP-*b*-PCL, a broad exothermic peak associated with the sPP crystallization was identified at 64 °C in the cooling scan [cf. Figure 13a]. The sharp exotherm at 32.7 °C caused by the PCL crystallization was observed upon further cooling. The crystallization temperature of sPP block was depressed by 16 °C compared to that of the corresponding sPP homopolymer (i.e., sPP (2430)), showing that the crystallization of sPP block was highly confined by the cylindrical microdomain.[63]

For sPP-*b*-PLA the crystallization temperature of sPP block was only slightly lower than that of the corresponding sPP homopolymer, because sPP block now became the major component forming the continuous matrix. The slight depression (∼4 °C) of crystallization rate should be attributed to the restriction in molecular motion imposed by the covalent linkage of sPP block to PLA block.

Conclusions

This study has disclosed an effective synthetic method for successful preparations of structurally well-defined stereoregular diblock copolymers composing of syndiotactic polypropylene and polyesters (i.e., sPP-*b*-PCL and sPP-*b*-PLA) through the controlled ring-opening block copolymerization of cyclic esters using the aluminum alkoxide end-capped sPP as the macroinitiator. The aluminum alkoxide-terminated sPP macroinitiator was generated by activation of the OH-capped sPP with TEA, whereas the OH-capped sPP was produced by the selective chain transfer to TEA while conducting the syndiospecific propylene polymerization in the presence of *ansa*-metallocene catalysts. This study not only provided effective synthetic methods for the preparation of structurally well-define stereoregular BCPs for self-assembled nanopatterns but also presented the connection of the stereoregular polyolefins with polyesters in the second block. Moreover, since the stereoregular polyolefin-based macroinitiator (i.e., aluminum alkoxide end-capped sPP) was used

for the construction of second polymer blocks by the controlled ring-opening polymerization, the problems confronted in the anionic coupling block copolymerization using excess living homopolymer were circumvented. The structural characterizations revealed that hexagonally packed cylinder structures were formed through the microphase separations of the sPP-*b*-PCL and sPP-*b*-PLA in the melt state. The self-assembled nanostructures from the BCPs with the combination of the high solvent-resistance offered by the crystallizable sPP block and the polarity of the polyester block may be very appealing in the demands of new nanomaterials for a variety of applications.

Acknowledgment. J.-C.T. and H.-L.C. acknowledge the National Science Council of Taiwan for the financial support for this research under Contracts NSC 96-2216E-194-003 and NSC 97-2221-E-007-034-MY, respectively.

Supporting Information Available: Figures showing ^{13}C and ^{13}C(DEPT-135) and two-dimensional $^{1}H-^{1}H$ COSY and $^{1}H-^{13}C$ HMQC NMR spectra of the OH-capped sPP. This material is available free of charge via the Internet at http://pubs.acs.org.

References and Notes

(1) (a) Lazzari, M.; Liu, G.; Lecommandoux, S. *Block Copolymers in Nanoscience*; Wiley-VCH Verlag GmbH & Co. KGaA: Weinheim, Germany, 2006. (b) Abetz, V.; Hadjichristidis, H.; Iatrou, H.; Pitsikalis, M.; Simon, P. F. W. *Adv. Polym. Sci.* **2005**, *189*, 1–124. (c) Hadjichristidis, N.; Pispas, S.; Floudas, G. *Block Copolymers: Synthetic Strategies, Physical Properties and Applications*; John Wiley and Sons: New York, 2003. (d) Alexandridis, P.; Lindman, B. *Amphiphilic Block Copolymers: Self-Assembly and Applications*; Elsevier: Amsterdam, 2000. (e) Calleja, F. J. B.; Roslaniec, J. *Block Copolymers*; Marcel Dekker: New York, 2000.

(2) (a) Park, M.; Harrison, C.; Chaikin, P. M.; Register, R. A.; Adamson, D. H. *Science* **1997**, *276*, 1401–1404. (b) Huang, E.; Rockford, L.; Russell, T. P.; Hawker, C. J. *Nature (London)* **1998**, *395*, 757. (c) Zalusky, A. S.; Olayo-Valles, R.; Taylor, C. J.; Hillmyer, M. A. *J. Am. Chem. Soc.* **2001**, *123*, 1519–1520.

(3) (a) Bates, F. S.; Fredrickson, G. H. *Annu. Rev. Phys. Chem.* **1990**, *41*, 525–557. (b) Bates, F. S.; Fredrickson, G. H. *Phys. Today* **1999**, *52*, 32–38.

(4) (a) Whitesides, G. M.; Grzybowski, B. *Science* **2002**, *295*, 2418–2421. (b) De Rosa, C.; Park, C.; Thomas, E. L.; Lotz, B. *Nature (London)* **2000**, *405*, 433–437. (c) Ho, R.-M.; Hsieh, P.-Y.; Tseng, W.-H.; Lin, C. C.; Huang, B. H. *Macromolecules* **2003**, *36*, 9085–9092.

(5) (a) Zhu, L.; Mimnaugh, B. R.; Ge, Q.; Quirk, R. P.; Cheng, S. Z. D.; Thomas, E. L.; Lotz, B.; Hsiao, B. S.; Yeh, F.; Lin, L. *Polymer* **2001**, *42*, 9121–9131. (b) Ryan, A. J.; Hamley, I. W.; Bras, W.; Bates, F. S. *Macromolecules* **1995**, *28*, 3860–3868. (c) Zhu, L.; Chen, Y.; Zhang, A.; Calhoun, B. H.; Chun, M.; Quirk, R. P.; Cheng, S. Z. D.; Hsiao, B. S.; Yeh, F.; Hashimoto, T. *Phys. Rev. B* **1999**, *60*, 10022–10031.

(6) Nojima, S.; Kato, K.; Yamamoto, S.; Ashida, T. *Macromolecules* **1992**, *25*, 2237–2242.

(7) Richardson, P. H.; Richards, R. W.; Blundell, D. J.; MacDonald, W. A.; Mills, P. *Polymer* **1995**, *36*, 3059–3069.

(8) Hamley, I. W.; Fairclough, J. P. A.; Terrill, N. J.; Ryan, A. J.; Lipic, P. M.; Bates, F. S.; Towns-Andrews, E. *Macromolecules* **1996**, *29*, 8835–8843.

(9) Ryan, A. J.; Fairclough, J. P. A.; Hamley, I. W.; Mai, S. M.; Booth, C. *Macromolecules* **1997**, *30*, 1723–1727.

(10) Loo, Y. L.; Register, R. A.; Ryan, A. J. *Macromolecules* **2002**, *35*, 2365–2374.

(11) Weimann, P. A.; Hajduk, P. A.; Hajduk, D. A.; Chu, C.; Chaffin, K. A.; Brodil, J. C.; Bates, F. S. *J. Polym. Sci., Part B: Polym. Phys.* **1999**, *37*, 2053–2068.

(12) Arnal, M. L.; Balsamo, V.; Lopez-Carrasquero, F.; Contreras, J.; Carrillo, M.; Schmalz, H.; Abetz, V.; Laredo, E.; Müller, A. J. *Macromolecules* **2001**, *34*, 7973–7982.

(13) Chen, H. L.; Hsiao, S. C.; Lin, T. L.; Yamauchi, K.; Hasegawa, H.; Hashimoto, T. *Macromolecules* **2001**, *34*, 671–674.

(14) Nojima, S.; Toei, M.; Hara, S.; Tanimoto, S.; Sasaki, S. *Polymer* **2002**, *43*, 4087–4090.

(15) Albuerne, J.; Márquez, L.; Müller, A. J.; Raquez, J.-M.; Degée, Ph.; Dubois, Ph.; Castelletto, V.; Hamley, I. *Macromolecules* **2003**, *36*, 1633–1644.

(16) Loo, Y. L., Register, R. A. Crystallisation within block copolymers mesophases. In *Development in block copolymer science and technology*; Hamley, I. W., Ed.; John Wiley & Sons, Ltd.: London, 2004, pp 213.

(17) Müller, A. J.; Balsamo, V.; Arnal, M. L. *Adv. Polym. Sci.* **2005**, *190*, 1–63.

(18) Hamley, W.; Castelletto, V.; Castillo, R. V.; Müller, A. J.; Martin, C. M.; Pollet, E.; Dubois, Ph. *Macromolecules* **2005**, *38*, 463–472.

(19) Nojima, S.; Akutsu, Y.; Akaba, M.; Tanimoto, S. *Polymer* **2005**, *46*, 4060–4067.

(20) Takeshita, H.; Fukumoto, K.; Ohnishi, T.; Ohkubo, T.; Miya, M.; Takenaka, K.; Shiomi, T. *Polymer* **2006**, *47*, 8210–8218.

(21) Müller, A. J.; Balsamo, V.; Arnal, M. L. In *Lecture Notes in Physics: Progress in Understanding of Polymer Crystallization*; Reiter, G., Strobl, G., Eds.; Lecture Notes in Physics 714; Springer: Berlin, Germany, 2007; pp 229−259.

(22) Castillo, R. V.; Müller, A. J.; Lin, M. C.; Chen, H. L.; Jeng, U.-S.; Hillmyer, M. A. *Macromolecules* **2008**, *41*, 6154–6164.

(23) (a) Green, M. M.; Peterson, N. C.; Sato, T.; Teramoto, A.; Cook, R.; Lifson, S. *Science* **1995**, *268*, 1860–1866. (b) Palmans, A. R. A.; Meijer, E. W. *Angew. Chem., Int. Ed. Engl.* **2007**, *46*, 8948–8968. (c) Ho, R.-M.; Chung, T.-M.; Tsai, J.-C.; Kuo, J.-C.; Hsiao, B. S.; Sics, I. *Macromol. Rapid Commum.* **2005**, *26*, 107–111. (d) Chung, T.-M.; Ho, R.-M.; Kuo, J.-C.; Tsai, J.-C.; Hsiao, B. S.; Sics, I. *Macromolecules* **2006**, *39*, 2739–2742. (e) Ho, R.-M.; Chiang, Y.-W.; Tsai, C.-C.; Lin, C.-C.; Ko, B.-T.; Huang, B.-H. *J. Am. Chem. Soc.* **2004**, *126*, 2704–2705.

(24) (a) Hatada, K.; Kitayama, T.; Ute, K.; Nishiura, T. *Macromol. Rapid Commun.* **2004**, *25*, 1447–1477. (b) Tian, J.; Hustad, P. D.; Coates, G. W. *J. Am. Chem. Soc.* **2001**, *123*, 5134–5135. (c) Ruokolainen, J.; Mezzenga, R.; Fredrickson, G. H.; Kramer, E. J.; Hustad, P. D.; Coates, G. W. *Macromolecules* **2005**, *38*, 851–860.

(25) (a) Kandil, U.; Chung, T. C. *J. Polym. Sci., Part A: Polym. Chem.* **2005**, *43*, 1858–1872. (b) Dong, J. Y.; Wang, Z. M.; Hong, H.; Chung, T. C. *Macromolecules* **2002**, *35*, 9352–9359. (c) Lu, Y.; Hu, Y.; Wang, Z. M.; Manuas, E.; Chung, T. C. *J. Polym. Sci., Part A: Polym. Chem.* **2002**, *40*, 3416–3425. (d) Amin, S. B.; Marks, T. J. *J. Am. Chem. Soc.* **2007**, *129*, 2938–2953. (e) Mogstad, A.-L.; Waymouth, R. M. *Macromolecules* **1994**, *27*, 2313–2315. (f) Xu, G.; Chung, T. C. *Macromolecules* **1999**, *32*, 8689–8692. (g) Chung, T. C.; Dong, J. Y. *J. Am. Chem. Soc.* **2001**, *123*, 4871–4876. (h) Lin, W.; Dong, J.; Chung, T. C. M. *Macromolecules* **2008**, *41*, 8452–8457.

(26) (a) Kuo, J.-C.; Tsai, J.-C.; Chung, T.-M.; Ho, R.-M. *Macromolecules* **2006**, *39*, 7520–7526. (b) Lin, W.-F.; Tsai, J.-C. *J. Polym. Sci., Part A: Polym. Chem.* **2008**, *46*, 2167–2176. (c) Lin, W.-F.; Hsiao, T.-J.; Tsai, J.-C.; Chung, T.-M.; Ho, R.-M. *J. Polym. Sci., Part A: Polym. Chem.* **2008**, *46*, 4843–4856. (d) Kuo, J.-C.; Lin, W.-F.; Yu, C.-H.; Tsai, J.-C.; Wang, T.-C.; Chung, T.-M.; Ho, R.-M. *Macromolecules* **2008**, *41*, 7967–7977.

(27) (a) Ropson, N.; Dubois, P.; Jérôme, R.; Teyssie, P. *Macromolecules* **1995**, *28*, 7589–7598. (b) Kurcok, P.; Dubois, P.; Sikorska, W.; Jedlinski, Z.; Jérôme, R. *Macromolecules* **1997**, *30*, 5591–5595. (c) Carter, K. R.; Richter, R.; Kricheldorf, H. R.; Hedrick, J. L. *Macromolecules* **1997**, *30*, 6074–6076. (d) Kowalski, A.; Duda, A.; Penczek, S. *Macromolecules* **1998**, *31*, 2114–2122. (e) Kowalski, A.; Duda, A.; Penczek, S. *Macromol. Rapid Commun.* **1998**, *19*, 567–572. (f) Wang, H.; Dong, J.; Qiu, K. *J. Polym. Sci., Part A: Polym. Chem.* **1998**, *36*, 695–702. (g) Kim, C.; Lee, S.; Shin, J.; Yoon, J. *Macromolecules* **2000**, *33*, 7448–7452.

(28) (a) Wu, B.; Harlan, C. J.; Lenz, R. W.; Barron, A. R. *Macromolecules* **1997**, *30*, 316–318. (b) Scherman, O. A.; Rutenberg, I. M.; Grubbs, R. H. *J. Am. Chem. Soc.* **2003**, *125*, 8515–8522.

(29) (a) Razavi, A.; Ferrara, J. *J. Organomet. Chem.* **1992**, *435*, 299–310. (b) Resconi, L.; Piemontesi, F.; Gamurati, I.; Sudmeijer, O.; Nifant'ev, I. E.; Ivchenko, P. V.; Kuz'mina, L. G. *J. Am. Chem. Soc.* **1998**, *120*, 2308–2321.

(30) Patsidis, K.; Alt, G. H.; Milius, W.; Palackal, S. J. *J. Organomet. Chem.* **1996**, *509*, 63–71.

(31) Hasan, T.; Ioku, A.; Nishii, K.; Shiono, T.; Ikeda, T. *Macromolecules* **2001**, *34*, 3142–3145.

(32) Hu, Y.; Krejchi, M. T.; Shah, C. D.; Myers, C. L.; Waymouth, R. M. *Macromolecules* **1998**, *31*, 6908–6916.

(33) (a) Zambelli, A.; Locatelli, T.; Provasoli, A.; Ferro, D. R. *Macromolecules* **1980**, *13*, 267–270. (b) Veghini, D.; Henling, L. M.; Burkhardt, T. J.; Bercaw, J. E. *J. Am. Chem. Soc.* **1999**, *121*, 564–573.

(34) Han, C. J.; Lee, M. S.; Byun, D.-J.; Kim, S. Y. *Macromolecules* **2002**, *35*, 8923–8925.

(35) (a) Resconi, L.; Cavallo, L.; Fait, A.; Piemontesi, F. *Chem. Rev.* **2000**, *100*, 1253–1346. (b) Busico, V.; Cipullo, R.; Chadwick, J. C.; Modder, J. F.; Sudmeijer, O. *Macromolecules* **1994**, *27*, 7538–7543.

(36) (a) Lynd, N. A.; Hillmyer, M. A. *Macromolecules* **2005**, *38*, 8803–8810. (b) Lynd, N. A.; Hillmyer, M. A. *Macromolecules* **2007**, *40*, 8050–8055. (c) Lynd, N. A.; Meuler, A. J.; Hillmyer, M. A. *Prog. Polym. Sci.* **2008**, *33*, 875–893.

(37) (a) Schmidt, S. C.; Hillmyer, M. A. *Macromolecules* **1999**, *32*, 4794–4801. (b) Wang, Y.; Hillmyer, M. A. *Macromolecules* **2000**, *33*, 7395–7403. (c) Zalusky, A. S.; Olayo-Valles, R.; Wolf, J. H.; Hillmyer, M. A. *J. Am. Chem. Soc.* **2002**, *124*, 12761–12773.
(38) Maier, R.-D.; Thomann, R.; Kressler, J.; Mülhaupt, R.; Rudolf, B. *J. Polym. Sci., Part B: Polym. Phys.* **1997**, *35*, 1135–1144.
(39) Small, P. A. *J. Appl. Chem.* **1953**, *3*, 71–80.
(40) Blümm, E.; Owen, A. J. *Polymer* **1995**, *36*, 4077–4081.
(41) (a) Leibler, L. *Macromolecules* **1980**, *13*, 1602–1617. (b) Matsen, M. W.; Bates, F. S. *Macromolecules* **1996**, *29*, 1091.
(42) Förster, S.; Timmann, A.; Schellbah, C.; Meyer, A.; Funari, S. S.; Mulvaney, P.; Knott, R. *J. Phys. Chem. B* **2005**, *109*, 1347–1360.
(43) Rangarajan, P.; Register, R. A.; Fetters, L. J. *Macromolecules* **1993**, *26*, 4640–4645.
(44) Floudas, G.; Ulrich, R.; Wiesner, U. *J. Chem. Phys.* **1999**, *110*, 652–663.
(45) De Rosa, C.; Auriemma, F. *Prog. Polym. Sci.* **2006**, *31*, 145–237.
(46) Supaphol, P. *J. Appl. Polym. Sci.* **2001**, *82*, 1083–1097.
(47) Boor, J.; Youngman, E. A. *J. Polym. Sci., Part B: Polym. Lett.* **1965**, *3*, 577–580.
(48) Youngman, E. A.; Boor, J. *Macromol. Rev.* **1967**, *2*, 33–69.
(49) Supaphol, P. *J. Appl. Polym. Sci.* **2000**, *78*, 338–354.
(50) Supaphol, P.; Thanomkiat, P.; Phillips, R. *Polym. Test.* **2004**, *23*, 881–895.
(51) Marchetti, A.; Martuscelli, E. *J. Polym. Sci., Part B: Polym. Phys.* **1974**, *12*, 1649–1666.
(52) Rodriguez-Arnold, J.; Zhang, A.; Cheng, S. Z. D.; Lovinger, A.; Hsieh, E. T.; Chu, P.; Johnson, T. W.; Honnell, K. G.; Geerts, R. G.; Palackal, S. J.; Hawley, G. R.; Welch, M. B. *Polymer* **1994**, *35*, 1884–1895.
(53) Holdsworth, P. J.; Turner-Jones, A. *Polymer* **1971**, *12*, 195–208.
(54) Lee, Y. C.; Porter, R. S. *Macromolecules* **1987**, *20*, 1336–1341.
(55) Jonas, A. M.; Russell, T. P.; Yoon, D. *Macromolecules* **1995**, *28*, 8491–8503.
(56) Lattimer, M. P.; Hobbs, J. K.; Hill, M. J.; Barham, P. J. *Polymer* **1992**, *33*, 3971–3973.
(57) Krüger, K.-N.; Zachmann, H. G. *Macromolecules* **1993**, *26*, 5202–5208.
(58) Hsiao, B. S.; Gardner, K. H.; Wu, D. Q.; Chu, B. *Polymer* **1993**, *34*, 3986–3995.
(59) Hsiao, B. S.; Gardner, K. H.; Wu, D. Q.; Chu, B. *Polymer* **1993**, *34*, 3996–4003.
(60) Lovinger, A. J.; Davis, D. D.; Lotz, B. *Macromoelcules* **1991**, *24*, 552–560.
(61) Lovinger, A. J.; Lotz, B.; Davis, D. D.; Padden, F. J., Jr. *Macromolecules* **1993**, *26*, 3494–3503.
(62) Lovinger, A. J.; Lotz, B.; Davis, D. D. *Polymer* **1990**, *31*, 2253–2259.
(63) Chen, H. L.; Wu, J. C.; Lin, T. L.; Lin, J. S. *Macromolecules* **2001**, *34*, 6936–6944.

MA802598N